Estimation of Tire–Road Friction Based on Onboard 6-DoF Acceleration Measurement

Chang-Sei Kim, *Member, IEEE*, Jin-Oh Hahn, *Member, IEEE*,
Keum-Shik Hong, *Senior Member, IEEE*, and Wan-Suk Yoo

Abstract—This paper presents a tire–road friction coefficient estimation method based on the six-degrees-of-freedom (6-DoF) vehicle body acceleration. The key principle of the proposed method is to estimate the tire–road friction coefficient from the accelerations at the tire. A vehicle model is applied to the 6-DoF vehicle body acceleration to derive longitudinal, lateral, and normal accelerations at each tire. Then, the recursive least squares (RLS) method is applied to the accelerations thus derived to estimate the tire–road friction coefficient. The main advantage of the proposed method is that it can be implemented with a 6-DoF accelerometer, which may be available in today's passenger vehicles equipped with accelerometers and gyroscopes. The method was validated with experiments in a passenger sedan, which demonstrates that the method is able to estimate tire–road friction coefficients accurately in real time during longitudinal emergency braking.

Index Terms—Accelerometer, friction model, system identification, tire–road friction coefficient, vehicle dynamics.

I. Introduction

TODAY'S vehicles are routinely equipped with advanced safety systems such as antilock braking systems, traction control systems, vehicle stability control systems, and unified chassis control systems. These systems manipulate tire forces to control dynamic vehicle motion (see, e.g., [1]–[8]). Ideally, therefore, proper functioning of these safety systems requires highly accurate tire force measurement.

Perhaps the most important parameter in determining tire force is the tire–road friction coefficient [9]–[11]. It is well known that longitudinal and lateral tire forces are largely affected by the friction coefficient at the tire–road interface in that it essentially determines the maximum tire forces available to vehicle safety systems [12], [13]. For example, the vehicle is difficult to stabilize in the case that tire–road friction coefficients at individual tires are largely different since the amount of available tire forces at each tire will be different. Therefore, the availability of tire–road friction coefficient can significantly benefit today's vehicle safety systems. Unfortu-

nately, however, there is literally no practical onboard sensor technology available that can measure tire forces and tire–road friction coefficients.

To resolve the above challenge, there has been significant interest in developing methods to indirectly estimate tire–road friction coefficient, as evidenced by a large volume of previous studies (see, e.g., [9], [14]–[18]). Many existing methods are built upon tire–road friction models that represent the friction characteristics on the tire–road interface. These friction models are classified into static and dynamic models [19]. Static models are characterized by Coulomb friction, viscosity, and stiction [20]. Dynamic models are represented by partial differential equations describing the characteristics of tire and road surfaces. Dahl's model [21], the Bristle model [22], the LuGre model [23], and the Dugoff model [24] are the most frequently used dynamic models. Based on the above wide-ranging tire–road friction models, often combined with vehicle dynamics models, a variety of methods to estimate tire–road friction coefficient have been reported in the literature. Alvarez *et al.* [10] proposed an adaptive observer to estimate tire–road friction from longitudinal acceleration based on a modified lumped LuGre model. Doumiati [25] developed two observers based on a simplified four-wheel-vehicle model and a modified quasi-static Dugoff model to estimate tire force and slip angle. Ray [26] proposed a nonlinear state estimator for the bicycle model based on the extended Kalman filter (EKF). Later, she developed an estimator for tire force and friction applicable to a full vehicle model. Hahn *et al.* [15] proposed a GPS-based method to estimate tire–road friction coefficient. Grip *et al.* [17] designed a nonlinear observer for estimating vehicle sideslip based on a rigid-body planar model of the vehicle. Matuško *et al.* [27] developed a neural-network-based method to estimate tire–road friction based on the lumped LuGre model. Kim [28] proposed an EKF-based method to estimate lateral tire forces. Cho *et al.* [29] proposed to estimate longitudinal and lateral tire forces by integrating longitudinal and planar vehicle models and utilizing shaft torque derived from onboard sensor measurements. It is obvious that the efficacy of these methods hinges upon the fidelity of tire–road friction model. Since the interaction between tire and road surface is highly complex and nonlinear [30], low-order tire–road friction models appropriate for designing advanced observers, and state-of-the-art signal processing techniques may inevitably suffer from errors, which may in turn deteriorate the accuracy of the tire–road friction coefficient. In the ideal, tire–road friction coefficient must be estimated directly from onboard sensor measurements with no additional state/parameter estimation
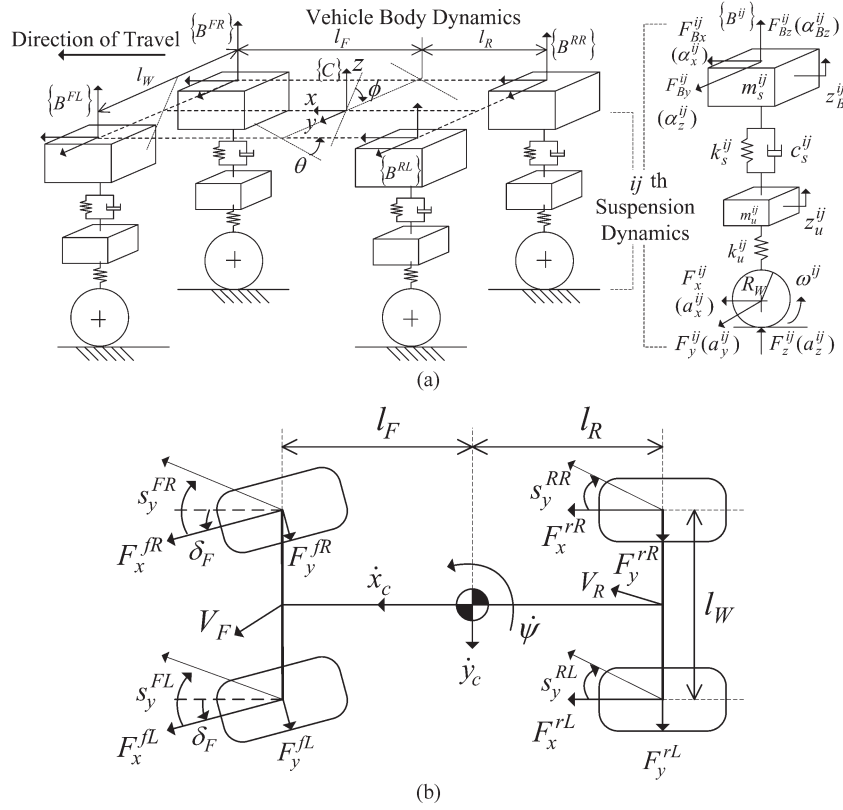
Fig. 1. Schematic of vehicle model with suspension dynamics. (a) Full vertical vehicle model. (b) Three-DoF planar vehicle model.

procedures involving these potentially erroneous tire–friction models.

In this paper, we propose a real-time tire–road friction coefficient estimation method based on the six-degrees-of-freedom (6-DoF) vehicle body acceleration. The key principle of the proposed method is to estimate the tire–road friction coefficient from the accelerations at the tire. A vehicle model is applied to the 6-DoF vehicle body acceleration to derive longitudinal, lateral, and normal accelerations at each tire. Specifically, longitudinal and lateral tire accelerations are derived using kinematic and dynamic vehicle models, whereas normal tire acceleration is derived by analyzing normal vehicle body acceleration using a blackbox model describing the dynamics of suspension and tire. Then, the recursive least squares (RLS) method is applied to the accelerations thus derived to estimate the tire–road friction coefficient. The main advantage of the proposed method is that it can be implemented with a 6-DoF accelerometer, which may be available and can be widely utilized in today's passenger vehicles equipped with accelerometers and gyroscopes [31], [32]. The major contributions of this paper are the formalization and development of a novel low-cost acceleration-based tire–road friction coefficient estimation method, and its preliminary experimental validation under longitudinal emergency braking maneuvers.

This paper is organized as follows. Section II provides a high-level overview of the proposed tire–road friction coefficient estimation method. Section III describes the estimation of tire accelerations from onboard 6-DoF acceleration measurements, and Section IV details the estimation of tire–road friction coefficient at each tire from tire accelerations. The experimental

setup, procedure, and results are presented and discussed in Section V. This paper is concluded in Section VI.

II. METHOD OVERVIEW

The proposed tire–road friction coefficient estimation method is built upon a full vehicle model that is made up of four quarter-car models (see Fig. 1). The model incorporates all 6-DoF motions, including surge, sway, heave, pitch, yaw, and roll. Fig. 2 shows the operational diagram of the proposed tire–road friction coefficient estimation method. It is composed of three steps: 1) computation of normal, longitudinal, and lateral accelerations at four sprung mass locations $(B^{FR}, B^{FL}, B^{RR}, B^{RL})$ based on the 6-DoF accelerations at the vehicle's mass center; 2) computation of normal, longitudinal, and lateral accelerations at four tires (i.e., unsprung masses) from sprung mass accelerations; and 3) estimation of tire–road friction coefficients by processing the tire accelerations using a recursive estimation method. First, sprung mass accelerations are computed from 6-DoF accelerations at the vehicle's mass center via a kinematic vehicle model. Second, longitudinal and lateral tire accelerations are obtained by applying a coordinate transformation and the load transfer effects to their unsprung mass counterparts, whereas normal tire acceleration is obtained by transforming its sprung mass counterpart, compensated for load transfer, via a blackbox model describing the dynamics of suspension and tire. Third, recursive parameter estimation methods are applied to the tire accelerations to estimate the tire–road friction coefficients at individual tires. In this context, the tire–road friction coefficient, which is typically defined as
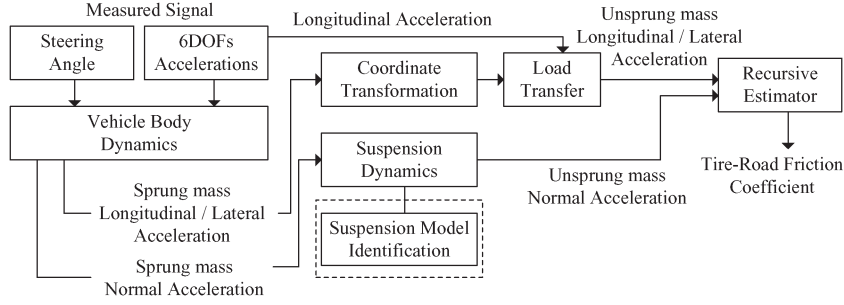
Fig. 2. Block diagram of the proposed tire–road friction coefficient estimation.

the ratio between planar and normal tire forces, is reformulated into the ratio between normal and planar tire accelerations, i.e.,

$$\mu_x^{ij} = \frac{F_x^{ij}}{F_z^{ij}} = \frac{a_x^{ij}}{a_z^{ij} + g}$$
$$\mu_y^{ij} = \frac{F_y^{ij}}{F_z^{ij}} = \frac{a_y^{ij}}{a_z^{ij} + g} \tag{1}$$

where μ_x^{ij} and μ_y^{ij} are longitudinal and lateral tire–road friction coefficients, respectively, at tire (i,j), $i \in \{F, R\}$, $j \in \{R, L\}$; F_x^{ij}, F_y^{ij}, and F_z^{ij} are the longitudinal, lateral and normal tire forces, respectively; and a_x^{ij}, a_y^{ij}, a_z^{ij} are the longitudinal, lateral, and normal tire accelerations; and g is the gravity acceleration constant. The main advantage in the above acceleration-based formulation of tire–road friction coefficient is that it yields tire–road friction coefficients directly from acceleration measurements without tire force estimation.

In the following, each of the aforementioned steps to estimate tire–road friction coefficient are discussed in detail.

III. ESTIMATION OF TIRE ACCELERATIONS

In the proposed method, sprung mass accelerations are first computed from the 6-DoF accelerations at the mass center of the vehicle, and then tire accelerations are computed from the sprung mass accelerations.

A. Sprung Mass Accelerations

Considering that the vehicle body (or chassis) is a rigid body, longitudinal, lateral, and normal accelerations at each quarter car's sprung mass due to the 6-DoF accelerations at the center of mass of the vehicle can be computed from the 6-DoF mass center accelerations using a kinematic vehicle model as follows. First, normal acceleration at each sprung mass is determined by the body's heave, pitch, and roll motions via superposition as follows:

$$\alpha_z^{FL} = \ddot{z}_c - l_F\ddot{\theta} + \frac{l_W}{2}\ddot{\phi}$$
$$\alpha_z^{FR} = \ddot{z}_c - l_F\ddot{\theta} - \frac{l_W}{2}\ddot{\phi}$$
$$\alpha_z^{RL} = \ddot{z}_c + l_R\ddot{\theta} + \frac{l_W}{2}\ddot{\phi}$$
$$\alpha_z^{RR} = \ddot{z}_c + l_R\ddot{\theta} - \frac{l_W}{2}\ddot{\phi} \tag{2}$$

where α_z^{ij} is the normal acceleration at sprung mass (i,j), $i \in \{F, R\}$, $j \in \{R, L\}$; $\ddot{z}_c$ is the normal acceleration at the vehicle's mass center; $\ddot{\theta}$ and $\ddot{\phi}$ are the pitch and roll accelerations at the vehicle's mass center, respectively; l_F and l_R are the distances from the vehicle's mass center to front and rear axles, respectively; and l_W is the track.

Second, longitudinal and lateral accelerations at each sprung mass are determined by the body's surge, sway, and yaw motions via superposition as follows, which also accommodates the Coriolis force due to the vehicle's planar velocities and yaw rate

$$\alpha_x^{FL} = \ddot{x}_c - \frac{l_W}{2}\ddot{\psi} + \dot{y}_c\dot{\psi}, \qquad \alpha_y^{FL} = \ddot{y}_c + l_F\ddot{\psi} - \dot{x}_c\dot{\psi}$$

$$\alpha_x^{FR} = \ddot{x}_c + \frac{l_W}{2}\ddot{\psi} + \dot{y}_c\dot{\psi}, \qquad \alpha_y^{FR} = \ddot{y}_c + l_F\ddot{\psi} - \dot{x}_c\dot{\psi}$$

$$\alpha_x^{RL} = \ddot{x}_c - \frac{l_W}{2}\ddot{\psi} + \dot{y}_c\dot{\psi}, \qquad \alpha_y^{RL} = \ddot{y}_c - l_R\ddot{\psi} - \dot{x}_c\dot{\psi}$$

$$\alpha_x^{RR} = \ddot{x}_c + \frac{l_W}{2}\ddot{\psi} + \dot{y}_c\dot{\psi}, \qquad \alpha_y^{RR} = \ddot{y}_c - l_R\ddot{\psi} - \dot{x}_c\dot{\psi} \tag{3}$$

where α_x^{ij} and α_y^{ij} are the longitudinal and lateral accelerations at sprung mass $(i,j), i \in \{F, R\}, j \in \{R, L\}$, respectively; $\ddot{x}_c$ and $\ddot{y}_c$, and $\dot{x}_c$ and $\dot{y}_c$ are the longitudinal and lateral accelerations and velocities at the vehicle's mass center, respectively; and $\ddot{\psi}$ and $\dot{\psi}$ are the yaw acceleration and yaw rate at the vehicle's mass center, respectively. These sprung mass accelerations are subsequently utilized to compute normal, longitudinal, and lateral accelerations at individual tires, as described in the following.

B. Effect of Load Transfer

The sprung mass accelerations computed above are essentially the acceleration of the center of mass of the vehicle reflected kinematically at the four sprung mass locations (B^{FR}, B^{FL}, B^{RR}, B^{RL}). Thus, the effect of load transfer due to planar accelerations is not included in (2) and (3). In fact, this is why the pairs α_x^{FL} and α_x^{RL}, α_x^{FR} and α_x^{RR}, α_y^{FL} and α_y^{FR}, and α_y^{RL} and α_y^{RR}, respectively, are identical to each other. To obtain the "effective" sprung mass accelerations that take load transfer due to planar accelerations into account, the sprung mass accelerations in (2) and (3) are modified to incorporate the load transfer effect as follows. The amount of normal load transfer due to longitudinal acceleration $\ddot{x}_c$ and

At [A]: $(M_s + M_u)\ddot{x}_c h = W_x(l_F + l_R)$ At [B]: $(M_s + M_u)\ddot{y}_c h = W_y l_W$
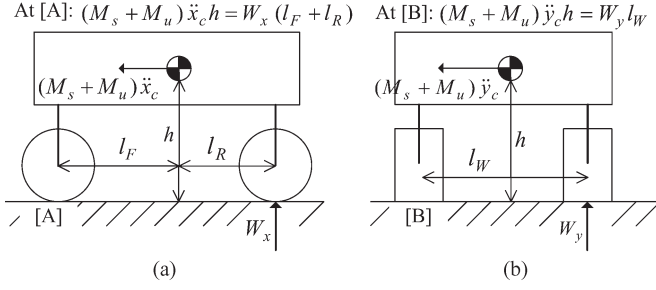

Fig. 3. Vehicle load transfer model. (a) Longitudinal load transfer. (b) Lateral load transfer.

lateral acceleration $\ddot{y}_c$ in a front-wheel-drive vehicle is given by (see Fig. 3)

$$W_x = (m_s + m_u)\ddot{x}_c \frac{h}{l_F + l_R} \quad W_y = (m_s + m_u)\ddot{y}_c \frac{h}{l_W} \quad (4)$$

where W_x and W_y are the amount of load transfer in longitudinal and lateral directions, respectively; m_s and m_u are the total sprung mass and unsprung mass of the vehicle, respectively; and h is the height of the mass center of the vehicle.

Since the consequence of the load transfer appears at the tire–road interface, it is the normal tire acceleration, not the normal sprung mass acceleration, which is directly altered by the load transfer. Accordingly, it is not straightforward to incorporate the effect of load transfer (4) into the normal sprung mass accelerations in (2) due to the presence of suspension dynamics (through which the two normal accelerations are related to each other). Therefore, we propose to adopt an empirical approach to incorporate the effect of load transfer on normal acceleration (as presented in Section III-C). In contrast, the effect of load transfer on longitudinal and lateral sprung mass accelerations (3) can be easily incorporated by recognizing that planar tire forces are proportionally related to normal tire forces by tire–road friction coefficient. Consider the following 2-DoF model of the suspension (see Fig. 1):

$$m_s^{ij}\alpha_z^{ij} = -c_s^{ij}\left(\int \alpha_z^{ij} - \int a_z^{ij}\right) - k_s^{ij}\left(\iint \alpha_z^{ij} - \iint a_z^{ij}\right)$$

$$m_u^{ij}a_z^{ij} = c_s^{ij}\left(\int \alpha_z^{ij} - \int a_z^{ij}\right) + k_s^{ij}\left(\iint \alpha_z^{ij} - \iint a_z^{ij}\right)$$

$$- k_u^{ij}\iint a_z^{ij} \quad (5)$$

where m_s^{ij} and m_u^{ij} are the sprung mass and unsprung mass, respectively; c_s^{ij} and k_s^{ij} are the suspension's damping and spring constants, respectively; k_u^{ij} is the tire stiffness; and a_z^{ij} is the normal acceleration of tire $(i,j), i \in \{F, R\}, j \in \{R, L\}$. Combining the above two equations yields the following expression for the dynamic tire force $\tilde{F}_z^{ij}, i \in \{F, R\}, j \in \{R, L\}$:

$$\tilde{F}_z^{ij} = -k_u \iint a_z^{ij} = m_s^{ij}\alpha_z^{ij} + m_u^{ij}a_z^{ij} \quad (6)$$

Thus, the total tire force $F_z^{ij}, i \in \{F, R\}, j \in \{R, L\}$, consisting of the static tire force due to the weight of the vehicle and the dynamic tire force due to vertical vehicle motion (6) is given by

$$F_z^{ij} = \bar{F}_z^{ij} + \tilde{F}_z^{ij} = \left(m_s^{ij} + m_u^{ij}\right)g + m_s^{ij}\alpha_z^{ij} + m_u^{ij}a_z^{ij}. \quad (7)$$

Note that (7) is the tire force when the vehicle is in purely vertical motion, i.e., it does not reflect the effect of load transfer. In the presence of longitudinal and lateral vehicle accelerations, the effective normal tire forces $\check{F}_z^{ij}, i \in \{F, R\}, j \in \{R, L\}$, can be written as follows based on (4) and (7):

$$\check{F}_z^{FL} = \left(m_s^{FL} + m_u^{FL}\right)g + m_s^{FL}\alpha_z^{FL} + m_u^{FL}a_z^{FL}$$
$$+ \frac{1}{2}(W_x + W_y)$$

$$\check{F}_z^{FR} = \left(m_s^{FR} + m_u^{FR}\right)g + m_s^{FR}\alpha_z^{FR} + m_u^{FR}a_z^{FR}$$
$$+ \frac{1}{2}(W_x - W_y)$$

$$\check{F}_z^{RL} = \left(m_s^{RL} + m_u^{RL}\right)g + m_s^{RL}\alpha_z^{RL} + m_u^{RL}a_z^{RL}$$
$$- \frac{1}{2}(W_x - W_y)$$

$$\check{F}_z^{RR} = \left(m_s^{RR} + m_u^{RR}\right)g + m_s^{RR}\alpha_z^{RR} + m_u^{RR}a_z^{RR}$$
$$- \frac{1}{2}(W_x + W_y). \quad (8)$$

Thus, the effective normal force at each tire can be obtained by multiplying the normal tire force (7) associated with purely vertical vehicle motion by a factor of $\check{F}_z^{ij}/F_z^{ij}$. Therefore, provided that suspension dynamics dominantly affect the normal (but not the planar) accelerations, the effective planar accelerations can also be computed by multiplying the planar tire accelerations (3) by a factor of $\check{F}_z^{ij}/F_z^{ij}$

$$\check{\alpha}_x^{FL} = \alpha_x^{FL}\frac{\check{F}_z^{FL}}{F_z^{FL}}$$
$$= \alpha_x^{FL}\left[1 + \frac{0.5(W_x + W_y)}{(m_s^{FL} + m_u^{FL})g + m_s^{FL}\alpha_z^{FL} + m_u^{FL}a_z^{FL}}\right]$$

$$\check{\alpha}_y^{FL} = \alpha_y^{FL}\frac{\check{F}_z^{FL}}{F_z^{FL}}$$
$$= \alpha_y^{FL}\left[1 + \frac{0.5(W_x + W_y)}{(m_s^{FL} + m_u^{FL})g + m_s^{FL}\alpha_z^{FL} + m_u^{FL}a_z^{FL}}\right]$$

$$\check{\alpha}_x^{FR} = \alpha_x^{FR}\frac{\check{F}_z^{FR}}{F_z^{FR}}$$
$$= \alpha_x^{FR}\left[1 + \frac{0.5(W_x - W_y)}{(m_s^{FR} + m_u^{FR})g + m_s^{FR}\alpha_z^{FR} + m_u^{FR}a_z^{FR}}\right]$$

$$\check{\alpha}_y^{FR} = \alpha_y^{FR}\frac{\check{F}_z^{FR}}{F_z^{FR}}$$
$$= \alpha_y^{FR}\left[1 + \frac{0.5(W_x - W_y)}{(m_s^{FR} + m_u^{FR})g + m_s^{FR}\alpha_z^{FR} + m_u^{FR}a_z^{FR}}\right]$$

$$\check{\alpha}_x^{RL} = \alpha_x^{RL}\frac{\check{F}_z^{RL}}{F_z^{RL}}$$
$$= \alpha_x^{RL}\left[1 - \frac{0.5(W_x - W_y)}{(m_s^{RL} + m_u^{RL})g + m_s^{RL}\alpha_z^{RL} + m_u^{RL}a_z^{RL}}\right]$$

$$\check{\alpha}_y^{RL} = \alpha_y^{RL}\frac{\check{F}_z^{RL}}{F_z^{RL}}$$

$$= \alpha_y^{RL} \left[1 - \frac{0.5(W_x - W_y)}{\left(m_s^{RL} + m_u^{RL}\right) g + m_s^{RL}\alpha_z^{RL} + m_u^{RL}a_z^{RL}} \right]$$

$$\breve{\alpha}_x^{RR} = \alpha_x^{RR} \frac{\breve{F}_z^{RR}}{F_z^{RR}}$$

$$= \alpha_x^{RR} \left[1 - \frac{0.5(W_x + W_y)}{\left(m_s^{RR} + m_u^{RR}\right) g + m_s^{RR}\alpha_z^{RR} + m_u^{RR}a_z^{RR}} \right]$$

$$\breve{\alpha}_y^{RR} = \alpha_y^{RR} \frac{\breve{F}_z^{RR}}{F_z^{RR}}$$

$$= \alpha_y^{RR} \left[1 - \frac{0.5(W_x + W_y)}{\left(m_s^{RR} + m_u^{RR}\right) g + m_s^{RR}\alpha_z^{RR} + m_u^{RR}a_z^{RR}} \right]. \tag{9}$$

The computation of these modified planar sprung mass accelerations is not trivial since the normal unsrpung mass (or tire) accelerations $a_z^{ij}, i \in \{F, R\}, j \in \{R, L\}$, cannot be directly measured. The proposed approach to resolve this challenge is outlined in Section III-C.

C. Tire Accelerations

Tire–road friction coefficient is defined in terms of normal and planar tire forces (or equivalently, normal and planar tire accelerations). Thus, the sprung mass accelerations computed above need to be translated to the tire (i.e., unsprung mass) accelerations.

The normal tire accelerations cannot be obtained from the 6-DoF acceleration measurement directly because normal motions associated with sprung mass [given in terms of the sprung mass accelerations (2)] and tire are related by the dynamics of suspension. Therefore, normal tire accelerations must be estimated from normal sprung mass acceleration through the dynamics of suspension. However, the normal sprung mass accelerations in (2) do not reflect the effect of load transfer due to longitudinal and lateral vehicle accelerations. We propose to incorporate the effect of load transfer into (2) empirically by stating that the effective normal sprung mass acceleration is given by a linear combination of normal sprung mass accelerations (2) plus the planar vehicle accelerations, i.e.,

$$\breve{\alpha}_z^{ij} = \alpha_z^{ij} + \eta_x^{ij}\ddot{x}_c + \eta_y^{ij}\ddot{y}_c \tag{10}$$

where $\breve{\alpha}_z^{ij}, i \in \{F, R\}, j \in \{R, L\}$, denote the (empirical) effective normal sprung mass accelerations, whereas η_x^{ij} and η_y^{ij} are the weights representing the impact of longitudinal and lateral load transfer (see Section V for how these values are determined).

The suspension dynamics sought in this paper are essentially the transfer function relating the effective sprung mass accelerations (10) to the effective dynamic tire accelerations $\breve{a}_z^{ij}, i \in \{F, R\}, j \in \{R, L\}$ and are expressed as follows based on (8):

$$\breve{a}_z^{ij} = \frac{\breve{F}_z^{ij}}{\left(m_s^{ij} + m_u^{ij}\right)} - g \tag{11}$$

Obviously, it is extremely difficult to derive such a transfer function from the traditional 2-DoF model of suspension (5) (see Fig. 1). Consequently, we propose to identify a blackbox model of the suspension from experimental data (see Section V for detail). The resulting transfer function, denoted by $H_{ij}(s)$, $i \in \{F, R\}, j \in \{R, L\}$, can readily yield an estimate of normal tire acceleration at each tire from the corresponding normal sprung mass acceleration

$$\breve{a}_z^{ij} = H_{ij}(s)\breve{\alpha}_z^{ij}. \tag{12}$$

These effective normal tire accelerations can then be used to aid in estimating the planar sprung mass accelerations (9). For example, for $i = F$ and $j = L$, (8) and (11) together yields

$$\underbrace{\left(m_s^{FL} + m_u^{FL}\right) g + m_s^{FL}\alpha_z^{FL} + m_u^{FL}a_z^{FL}}_{\breve{F}_z^{FL} - (W_x + W_y)/2}$$

$$= \underbrace{\left(m_s^{FL} + m_u^{FL}\right)\left(\breve{a}_z^{FL} + g\right)}_{\breve{F}_z^{FL}} - \frac{1}{2}(W_x + W_y). \tag{13}$$

Noting that the left-hand side of (13) is the denominator term in the multiplying factors for $\breve{\alpha}_x^{FL}$ and $\breve{\alpha}_y^{FL}$ in (9), the planar sprung mass accelerations $\breve{\alpha}_x^{FL}$ and $\breve{\alpha}_y^{FL}$ can be estimated from $\breve{a}_z^{FL}$ using (13). Other planar sprung mass accelerations in (9) can be estimated similarly.

In regard to effective longitudinal and lateral sprung mass accelerations (9), they need to be coordinate-transformed when translating into effective longitudinal and lateral tire accelerations due to steering angle; more specifically, longitudinal and lateral sprung mass accelerations must be rotated by the steering angle to yield the corresponding tire accelerations (see Fig. 1). Therefore, longitudinal and lateral tire accelerations can be computed from their sprung mass counterparts by

$$\begin{bmatrix} \breve{a}_x^{ij} \\ \breve{a}_y^{ij} \end{bmatrix} = \begin{bmatrix} \cos\delta_i & \sin\delta_i \\ -\sin\delta_i & \cos\delta_i \end{bmatrix} \begin{bmatrix} \breve{\alpha}_x^{ij} \\ \breve{\alpha}_y^{ij} \end{bmatrix} \tag{14}$$

where $\breve{a}_x^{ij}$ and $\breve{a}_y^{ij}$ are effective (meaning that the effect of load transfer is reflected) longitudinal and lateral accelerations at tire $(i, j), i \in \{F, R\}, j \in \{R, L\}$, and $\delta_i, i \in \{F, R\}$ are the steering angles associated with front and rear tires.

IV. TIRE–ROAD FRICTION COEFFICIENT ESTIMATION

Using normal, longitudinal, and lateral accelerations obtained in (12) and (14) for each tire, tire–road friction coefficient can be estimated at each tire by the acceleration-based model (1) with a_x^{ij}, a_y^{ij}, and a_z^{ij}, replaced by $\breve{a}_x^{ij}$, $\breve{a}_y^{ij}$, and $\breve{a}_z^{ij}$, respectively. However, direct algebraic computation of (1) may yield noise-corrupted tire–road friction coefficient estimate due to the measurement noise inherent in the acceleration variables. In addition, recursive evaluation of (1) is desired to track (potentially) time-varying changes in the tire–road friction coefficient. To enable noise-robust real-time estimation of tire–road friction coefficient, we propose to employ online estimation techniques. In particular, this paper employed the

RLS method and the recursive gradient method [33], [34] to estimate tire–road friction coefficients.

By regarding normal versus longitudinal and lateral tire accelerations as input and outputs, respectively, the following parametric model can be derived from (1)

$$\begin{bmatrix} \breve{a}_x^{ij} \\ \breve{a}_y^{ij} \end{bmatrix} = \begin{bmatrix} \mu_x^{ij} \\ \mu_y^{ij} \end{bmatrix} (\breve{a}_z^{ij} + g) = \theta^T \varphi \qquad (15)$$

where the unknown parameter $\theta = \begin{bmatrix} \mu_x^{ij} & \mu_y^{ij} \end{bmatrix}$ is the tire–road friction coefficient, and $\varphi = (\breve{a}_z^{ij} + g)$ is the regressor. Based on (15), the RLS estimator for longitudinal and lateral tire–road friction coefficients is given by

$$\begin{bmatrix} \hat{\mu}_x^{ij}(k) \\ \hat{\mu}_y^{ij}(k) \end{bmatrix} = \begin{bmatrix} \hat{\mu}_x^{ij}(k-1) \\ \hat{\mu}_y^{ij}(k-1) \end{bmatrix}$$
$$+ K(k) \left\{ \begin{bmatrix} \breve{a}_x^{ij}(k) \\ \breve{a}_y^{ij}(k) \end{bmatrix} - \begin{bmatrix} \hat{\mu}_x^{ij}(k-1) \\ \hat{\mu}_y^{ij}(k-1) \end{bmatrix} (\breve{a}_z^{ij}(k) + g) \right\} \quad (16a)$$

where $k \in \mathbb{Z}^+$ is the sample time step, and $K(k)$ is the update gain given by

$$K(k) = \frac{P(k-1) \cdot (\breve{a}_z^{ij}(k) + g)}{\lambda + P(k-1) \cdot (\breve{a}_z^{ij}(k) + g)^2} \qquad (16b)$$

and $P(k)$ is the covariance given by

$$P(k) = \frac{1}{\lambda} \left[P(k-1) - \frac{P^2(k-1) \cdot (\breve{a}_z^{ij}(k) + g)^2}{\lambda + (k-1) \cdot (\breve{a}_z^{ij}(k) + g)^2} \right] \tag{16c}$$

where λ is the forgetting factor, which is used to reduce the effect of old data that no longer represents the underlying process.

On the other hand, the gradient estimator (GE) for longitudinal and lateral tire–road friction coefficients is given by

$$\begin{bmatrix} \hat{\mu}_x^{ij}(k) \\ \hat{\mu}_y^{ij}(k) \end{bmatrix} = \left\{ I - \Gamma \left(\breve{a}_z^{ij}(k) + g \right)^2 \right\} \begin{bmatrix} \hat{\mu}_x^{ij}(k-1) \\ \hat{\mu}_y^{ij}(k-1) \end{bmatrix}$$
$$+ \Gamma \begin{bmatrix} \breve{a}_x^{ij}(k) \\ \breve{a}_y^{ij}(k) \end{bmatrix} (\breve{a}_z^{ij}(k) + g) \quad (17)$$

where $\Gamma = \begin{bmatrix} \gamma_x & 0 \\ 0 & \gamma_y \end{bmatrix}$ is the update gain matrix ($\gamma_x > 0$ and $\gamma_y > 0$).

Once longitudinal and lateral tire–road friction coefficients are made available from (16) or (17), the resultant tire–road friction coefficient is obtained as follows:

$$\hat{\mu}^{ij}(k) = \sqrt{\left[\hat{\mu}_x^{ij}(k) \right]^2 + \left[\hat{\mu}_y^{ij}(k) \right]^2}. \qquad (18)$$

Tire–road friction coefficient is dependent on tire slip [14]. Thus, comparing the relation between tire slip and tire–road friction coefficient determined by the proposed method with those that are found in the literature can be useful in establishing the validity of the proposed method. Both longitudinal and
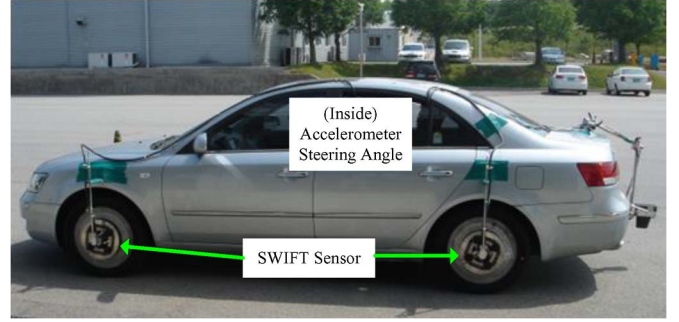

Fig. 4. Experimental setup for vehicle experiment.

lateral tire slips can be computed based on the 6-DoF acceleration measurements as follows:

$$s_x^{ij} = 1 - \frac{R_W \omega^{ij}}{V_i \cos s_y^{ij}}$$
$$s_y^{Fj} = \delta_F - \tan^{-1} \left(\frac{\dot{y}_c + l_F \dot{\psi}}{\dot{x}_c} \right)$$
$$s_y^{Rj} = - \tan^{-1} \left(\frac{\dot{y}_c - l_R \dot{\psi}}{\dot{x}_c} \right) \qquad (19a)$$

where s_x^{ij} and s_y^{ij} are longitudinal and lateral tire slips, respectively, at tire (i,j), $i \in \{F, R\}, j \in \{R, L\}$; R_W is the tire radius, ω^{ij} is the angular velocity of tire (i,j), and V_i is given by

$$V_F = \sqrt{(\dot{x}_c)^2 + (\dot{y}_c + l_F \dot{\psi})^2}$$
$$V_R = \sqrt{(\dot{x}_c)^2 + (\dot{y}_c - l_R \dot{\psi})^2}. \qquad (19b)$$

V. EXPERIMENTAL SETUP, PROCEDURES, AND RESULTS

To validate the proposed method for estimating tire–road friction coefficient, experimental data were collected from vehicle tests on dry asphalt roads. This section presents experimental setup and results in detail.

A. Experimental Setup and Procedures

A 6-DoF accelerometer and a steering angle encoder sensor were installed on a passenger sedan. In addition, SWIFT sensors [35] were attached to front left and rear left wheels to measure forces and moments acting on the tires and wheel angular velocities (see Fig. 4). On dry asphalt roads, data were collected at a sampling frequency of 1 kHz, whereas the vehicle was running with constant speeds at 40 and 60 km/h and then was stopped via strong emergency braking maneuver by a professional test driver. The 6-DoF acceleration data thus collected were processed by a Butterworth low-pass filter with cutoff frequency of 50 Hz to suppress the measurement noise.

The sprung mass accelerations were computed from the 6-DoF acceleration measurement at the vehicle's mass center via (2) and (3). These accelerations were transformed to incorporate the effect of load transfer by (10) and (9), respectively. These effective sprung mass accelerations were then translated

to the respective tire accelerations by (12) and (14). These tire accelerations were then processed by the RLS estimator (16) and the GE (17) to yield longitudinal and lateral tire–road friction coefficients. Finally, (18) was used to compute the resultant tire–road friction coefficient.

To compute normal tire acceleration from normal sprung mass acceleration, the suspension model $H(s)$ in (12) must be available. This model was determined from the data associated with 40-km/h experiment via parametric system identification technique and was subsequently validated with the data associated with 60-km/h experiment. Specifically, $H(s)$ was identified together with η_x^{ij} and η_y^{ij} so that the ∞-norm of the error between measured versus model-predicted normal tire accelerations in response to effective sprung mass acceleration were minimized as follows:

$$
\begin{aligned}
&\left\{ \left[\eta_x^{ij}\right]^*, \left[\eta_y^{ij}\right]^*, \left[\theta^{ij}\right]^* \right\} \\
&= \arg \min_{\eta_x^{ij}, \eta_y^{ij}, \theta^{ij}} \left\| \breve{a}_z^{ij}(k) - \mathcal{L}^{-1}\left[H_{ij}(s, \theta^{ij})\breve{\alpha}_z^{ij}(s) \right] \right\|_\infty \\
&= \arg \min_{\eta_x^{ij}, \eta_y^{ij}, \theta^{ij}} \\
&\quad \times \left\| \frac{\breve{F}_z^{ij}(k)}{\left(m_s^{ij} + m_u^{ij}\right)} - g - \mathcal{L}^{-1} \right. \\
&\quad \left. \times \left[H_{ij}(s, \theta^{ij}) \left\{ \alpha_z^{ij}(s) + \eta_x^{ij}\ddot{x}_c(s) + \eta_y^{ij}\ddot{y}_c(s) \right\} \right] \right\|_\infty
\end{aligned}
$$

(20)

where $\breve{F}_z^{ij}$ was measured at the front left and the rear left tires by the SWIFT sensors. To model the suspension dynamics as a 1-DoF system equipped with the unsprung mass, a second-order ARX model was used as expression for $H_{ij}(s)$. Since the experimental data had negligibly small lateral vehicle acceleration in comparison with its longitudinal counterpart, η_y^{ij} was set to zero in solving (20). It is noted that (20) reduces to a standard least squares problem to identify $H_{ij}(s)$ for a given value of η_x^{ij}. Thus, (20) was solved by optimizing η_x^{ij} so that the difference between the measured normal acceleration $\breve{a}_z^{ij}(k)$ and its model-predicted counterpart $\mathcal{L}^{-1}[H_{ij}(s, \theta^{ij})\breve{\alpha}_z^{ij}(s)]$ was minimized. To guarantee the stability of the ARX model, the coefficients of the denominator polynomial were constrained to have positive values. The optimal values of η_x^{ij} derived from (20) were $\eta_x^{FL} = 0.58$ and $\eta_x^{RL} = 0.22$.

B. Experimental Results

Fig. 5(a) shows longitudinal velocity, front and rear wheel velocities, and steering angle of the test vehicle associated with the 60-km/h experiment, and Fig. 5(b) shows the corresponding accelerations associated with the same experiment. The emergency braking maneuver started at ~9.5 s. It is noted that small perturbations in steering angle were observed after the initiation of emergency braking maneuver, which produced lateral tire forces via tire slip angles, thereby resulting in lateral tire accelerations [see the sway acceleration in Fig. 5(b)]. However, the lateral acceleration was very small compared with its longitudinal counterpart, as can be seen by comparing surge
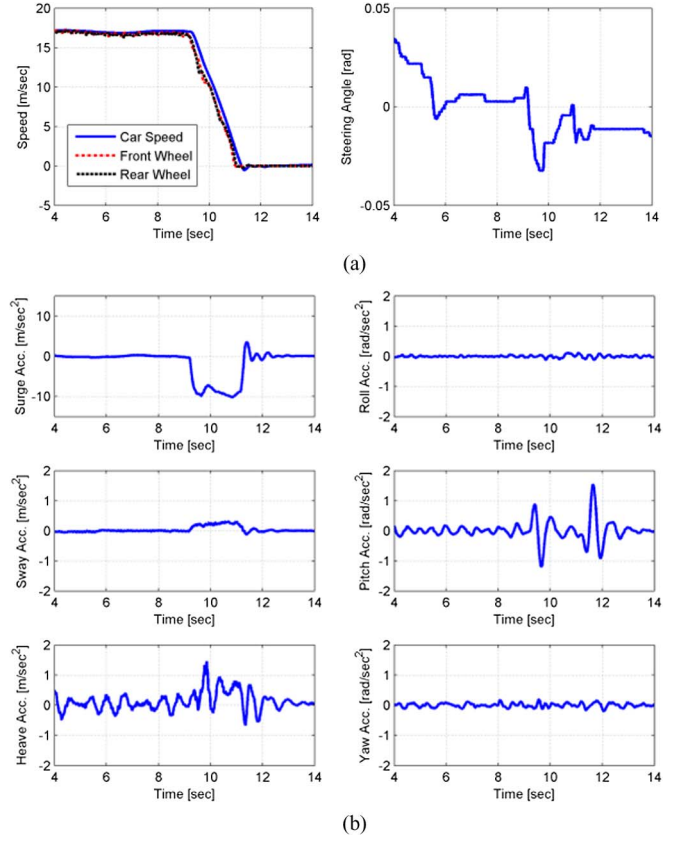

Fig. 5. Experiment data: 60-km/h experiment. (a) Measured vehicle velocity, front and rear wheel velocity, and steering angle. (b) Measured 6-DoF accelerations.
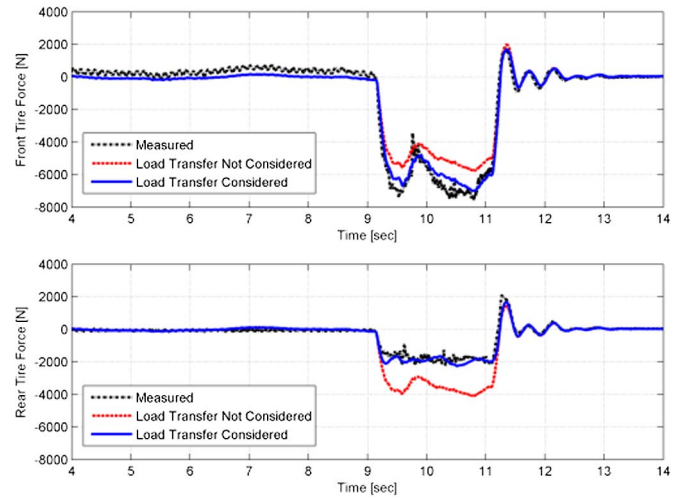

Fig. 6. Measured versus estimated longitudinal tire forces. In the time window of 2 s (between 9.2 s and 11.2 s to avoid dividing by zero tire forces while normalizing), the difference between measured versus estimated tire forces, normalized by the measured forces, was 21.2% (front) and 98.1% (rear) when the load transfer was not considered and 8.3% (front) and 12% (rear) when the load transfer was considered.

versus sway as well as pitch versus yaw. This well justifies the exclusion of the contributions from the lateral motion in determining the effective sprung mass accelerations in (20).

The longitudinal tire forces measured at the front left and the rear left tires are compared with those estimated by the proposed method in Fig. 6. The results clearly illustrate that 1) the effect of load transfer must be incorporated in estimating
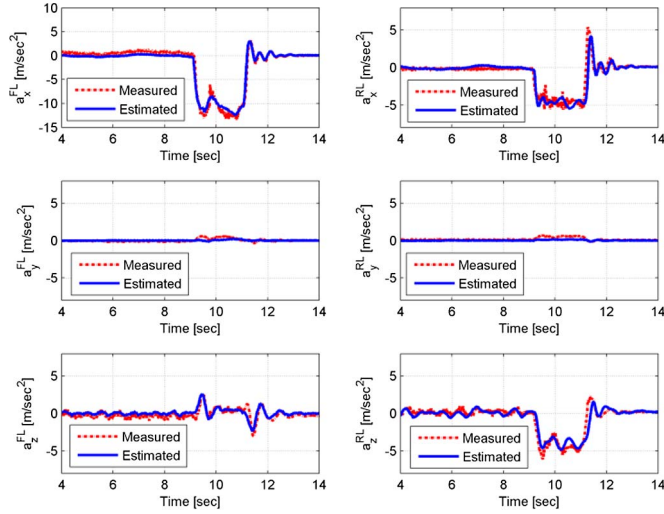
Fig. 7. Measured versus estimated accelerations at front left and rear left tires.
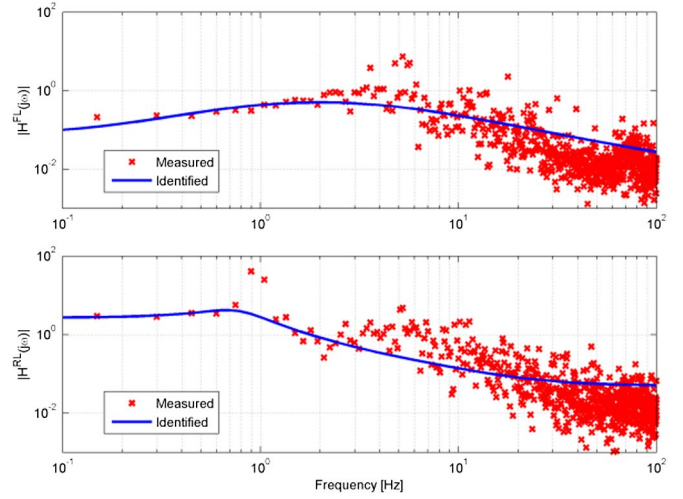

Fig. 8. Measured versus estimated frequency responses of front left (upper panel) and rear left (lower panel) suspensions.
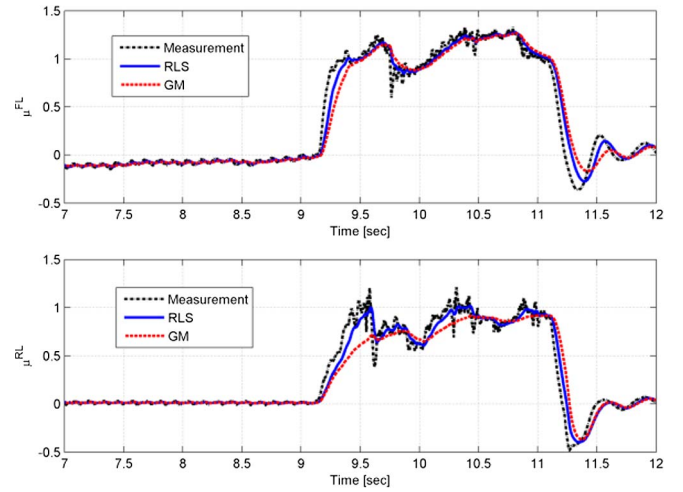

Fig. 9. Measured versus estimated tire–road friction coefficients at front left and rear left tires. RLS: recursive least squares estimator. GM: gradient estimator.

planar tire accelerations and that 2) the proposed approach (9) to accommodate the load transfer effect is valid.

Fig. 7 shows measured versus estimated tire accelerations at front left and rear left tires associated with 60-km/h experiment. Measured accelerations were derived by dividing the forces measured by the SWIFT sensors by the mass of the vehicle. Clearly, the tire accelerations estimated by the proposed method track their respective counterparts accurately. In particular, the accuracy of longitudinal and normal accelerations stands out. These results support the validity of the proposed approach to incorporate the effect of load transfer in deriving the effective normal and planar accelerations associated with both sprung masses and tires. In addition, the results also indicate that the blackbox model of suspension is a reasonable expression to relate the normal accelerations at the sprung mass to the tire. In particular, the frequency responses $H^{FL}(j\omega)$ and $H^{RL}(j\omega)$ of the suspensions associated with front left and rear left tires, which were identified from the data associated with the 40-km/h experiment, were notably consistent with their measured counterparts [given by the nonparametric transfer function estimates computed from the data of $\breve{\alpha}_z^{ij}(k)$ and $\breve{a}_z^{ij}(k)$] associated with the 60-km/h experiment (see Fig. 8), suggesting that the suspension model identified at a particular vehicle speed may be applicable to a reasonable range of vehicle speed.

Fig. 9 shows tire–road friction coefficients at front left and rear left tires computed for the 60-km/h experiment. First of all, the result indicated that recursive estimators were able to yield tire–road friction coefficients consistent with the measurements (i.e., tire–road friction coefficients computed by (1) based on normal and longitudinal tire forces measured by the SWIFT sensors). It is also noted that both tire–road friction coefficients were estimated to be very small during constant-speed driving (i.e., up to ∼9.5 s), whereas they were estimated to be as large as ∼1.3 and ∼1 for front and rear tires, respectively, during an emergency braking maneuver (i.e., between ∼9.5 s and ∼11 s). In fact, the values of longitudinal and lateral tire slips were very small (ranged between 0.02 and 0.03) during constant-speed driving, whereas their values assumed ∼0.9 and ∼0.1 during an emergency braking maneuver. Considering that the

tire–road friction coefficient is proportional to tire slip [14], the result presented in Fig. 9 can be deemed reasonable. It is also noted that the tire–road friction coefficients estimated for the right tires were highly consistent with those for the left tires (not shown).

Fig. 9 also compares tire–road friction coefficients derived directly from the 6-DoF acceleration measurements via (1) (denoted as "measurement"), RLS estimator via (16) and (18), and GE via (17) and (18). The result indicated that recursive estimators were effective in rejecting high-frequency fluctuations in tire–road friction coefficients that may have been caused by the noise in the 6-DoF acceleration measurements. In particular, RLS estimator showed superior speed of response than GE, which may be due to its time-varying adaptive gain. Noting that accurate real-time estimation of tire–road friction coefficient is crucial in deriving tire-slip-dependent tire–road friction characteristics (particularly the amount of slip where maximum tire force is attained), fast convergence of the estimates is of paramount importance in real time tire–road friction coefficient estimators.
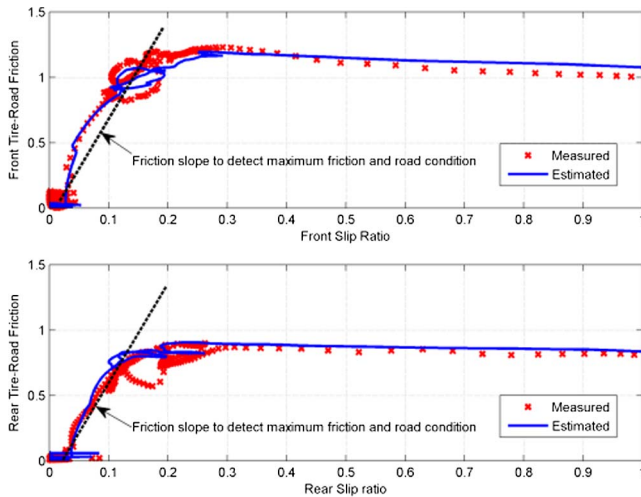
Fig. 10.   Measured versus estimated relation between tire slip and tire–road friction coefficient.

Fig. 10 presents the relation between tire slip and tire–road friction coefficient corresponding to front left (upper panel) and rear left (lower panel) tires, which strongly supports the validity of the proposed method in that the relation between tire slip and tire–road friction coefficient clearly shows the general trends anticipated from existing reports on tire–road friction coefficient models: tire–road friction coefficient increases with tire slip up to a threshold value, beyond which it decreases in response to increasing tire slip (e.g., [18] and [30]). The ability of the proposed method to derive the relation between tire slip and tire–road friction coefficient in real time can be useful in several ways, including, but not limited to 1) identifying maximum available tire force through maximum tire–road friction coefficient and 2) detecting road condition through computation of the slope between tire–road friction coefficient and tire slip [16], [36] (see Fig. 10).

C. Prospects and Limitations

A unique strength of the proposed method is that tire–road friction coefficient may be estimated by using 6-DoF acceleration measurements. Therefore, it may be easily deployed in today's passenger cars equipped with accelerometers and gyroscopes. However, there are a number of limitations in this paper, which requires further investigation. First, the experimental data were not ideal for comprehensive validation of the proposed method. In the lack of steering maneuver and widely varying velocities, the method was validated only at two different vehicle velocity regimes in which longitudinal accelerations were dominant but lateral accelerations were not large. For example, the validity of effective normal acceleration (10) in case both longitudinal and lateral accelerations are significantly large remains an open question. As well, the fidelity of the suspension model (12) under a wide range of vehicle velocities needs to be examined. Considering that empirical models must in general verified by extensive experiments, the validity of the empirical models (10) and (12) demonstrated in this paper based only on emergency braking on a straight road may not be generalizable to maneuvers involving large

accelerations in both the longitudinal and lateral directions. Future work on more rigorous validation of the proposed method with experimental data acquired from a wide range of driving maneuvers will be needed. Second, we derived longitudinal and lateral velocities in (3) by simply integrating the corresponding acceleration measurements due to the absence of interface with engine control unit. Noting that direct integration of acceleration measurements to derive velocities typically incurs biases and drifts, this may be responsible for some of the errors observed in our results. We expect that this problem may be resolved in actual implementation of the method since vehicle velocity can be measured or at least derived using the available onboard sensors (see, e.g., [37]–[39] for an example of estimating vehicle sideslip angle from onboard instrumentations, which can then be used to derive lateral velocity). In any case, since the proposed method is built upon acceleration measurements, which typically involve noise and artifact more severely than displacement and velocity measurements, robust sensor fusion and signal processing techniques will be beneficial in successfully implementing the proposed method.

VI. CONCLUSION

In this paper, a novel tire–road friction coefficient estimation method based on 6-DoF acceleration measurement has been proposed and validated under longitudinal emergency braking maneuvers. A tire–road friction coefficient model was formulated in terms of tire accelerations. These accelerations were computed by applying kinematic and dynamic vehicle models to accelerations measured at the vehicle's mass center, which were then used by the recursive estimators to determine tire–road friction coefficients in real time. Experimental results indicated that tire–road friction coefficient could be estimated by the proposed method accurately in real time during longitudinal emergency braking, and its relation to tire slip was consistent with the anticipated physical trends.

REFERENCES

[1] U. W. Kiencke and A. Daiss, "Estimation of tyre friction for enhanced ABS-systems," *JSAE Rev.*, vol. 16, no. 2, pp. 221–221, Apr. 1995.

[2] R. Rajamani, *Vehicle Dynamics and Control*. New York: Springer-Verlag, 2005.

[3] S. B. Choi, "Antilock brake system with a continuous wheel slip control to maximize the braking performance and the ride quality," *IEEE Trans. Control Syst. Technol.*, vol. 16, no. 5, pp. 996–1003, Sep. 2008.

[4] D. Piyabongkarn, R. Rajamani, J. A. Grogg, and J. Y. Lew, "Development and experimental evaluation of a slip angle estimator for vehicle stability control," *IEEE Trans. Control Syst. Technol.*, vol. 17, no. 1, pp. 78–88, Jan. 2009.

[5] J. Yoon, W. Cho, B. Koo, and K. Yi, "Unified chassis control for rollover prevention and lateral stability," *IEEE Trans. Veh. Technol.*, vol. 58, no. 2, pp. 596–609, Feb. 2009.

[6] G. Baffet, A. Charara, and D. Lechner, "Estimation of vehicle sideslip, tire force and wheel cornering stiffness," *Control Eng. Practice*, vol. 17, no. 11, pp. 1255–1264, Nov. 2009.

[7] C.-S. Liu and H. Peng, "Road friction coefficient estimation for vehicle path prediction," *Veh. Syst. Dyn.*, vol. 25, pp. 413–425, 1996.

[8] A. Mirzaei, M. Moallem, B. M. Dehkordi, and B. Fahimi, "Design of an optimal fuzzy controller for antilock braking systems," *IEEE Trans. Veh. Technol.*, vol. 55, no. 6, pp. 1725–1730, Nov. 2006.

[9] L. R. Ray, "Nonlinear tire force estimation and road friction identification: Simulation and experiments," *Automatica*, vol. 33, no. 10, pp. 1819–1833, Oct. 1997.

[10] L. Alvarez, J. Yi, R. Horowitz, and L. Olmos, "Dynamic friction model-based tire-road friction estimation and emergency braking control," *J. Dyn. Syst., Meas., Control*, vol. 127, no. 1, pp. 22–32, Jun. 2004.

[11] Y. Chen and J. Wang, "Adaptive vehicle speed control with input injections for longitudinal motion independent road frictional condition estimation," *IEEE Trans. Veh. Technol.*, vol. 60, no. 3, pp. 839–848, Mar. 2011.

[12] T. Hsiao, "Robust estimation and control of tire traction forces," *IEEE Trans. Veh. Technol.*, vol. 62, no. 3, pp. 1378–1383, Mar. 2013.

[13] G. A. Magallan, C. H. De Angelo, and G. O. Garcia, "Maximization of the traction forces in a 2WD electric vehicle," *IEEE Trans. Veh. Technol.*, vol. 60, no. 2, pp. 369–380, Feb. 2011.

[14] F. Gustafsson, "Slip-based tire-road friction estimation," *Automatica*, vol. 33, no. 6, pp. 1087–1099, Jun. 1997.

[15] J. O. Hahn, R. Rajamani, and L. Alexander, "GPS-based real-time identification of tire-road friction coefficient," *IEEE Trans. Control Syst. Technol.*, vol. 10, no. 3, pp. 331–343, May 2002.

[16] C. Lee, K. Hedrick, and K. Yi, "Real-time slip-based estimation of maximum tire-road friction coefficient," *IEEE/ASME Trans. Mechatronics*, vol. 9, no. 2, pp. 454–458, Jun. 2004.

[17] H. F. Grip *et al.*, "Nonlinear vehicle side-slip estimation with friction adaptation," *Automatica*, vol. 44, no. 3, pp. 611–622, Mar. 2008.

[18] R. Rajamani, G. Phanomchoeng, D. Piyabongkan, and J. Y. Lew, "Algorithms for real-time estimation of individual wheel tire-road friction coefficients," *IEEE/ASME Trans. Mechatronics*, vol. 17, no. 6, pp. 1183–1195, Dec. 2012.

[19] L. Li, F. Y. Wang, and Q. Zhou, "Integrated longitudinal and lateral tire/road friction modeling and monitoring for vehicle motion control," *IEEE Trans. Intell. Transp. Syst.*, vol. 7, no. 1, pp. 1–19, Mar. 2006.

[20] D. Karnopp, "Computer simulation of stick-slip friction in mechanical dynamic systems," *J. Dyn. Syst., Meas., Control*, vol. 107, no. 1, pp. 100–103, Mar. 1985.

[21] P. R. Dahl, "A solid friction model," Aerospace Corp., El Segundo, CA, USA, 1968.

[22] E. Denti and D. Fanteria, "Models of wheel contact dynamics: An analytical study on the in-plane transient responses of a brush model," *Veh. Syst. Dyn.*, vol. 34, no. 3, pp. 199–225, 2000.

[23] C. Canudas de Wit, H. Olsson, K. J. Astrom, and P. Lischinsky, "A new model for control of systems with friction," *IEEE Trans. Autom. Control*, vol. 40, no. 3, pp. 419–425, Mar. 1995.

[24] R. Guntar and S. Sankar, "A friction circle concept for Dugoff's tyre friction model," *Int. J. Veh. Des.*, vol. 1, no. 4, pp. 373–377, 1980.

[25] M. Doumiati, A. C. Victorino, A. Charara, and D. Lechner, "Onboard real-time estimation of vehicle lateral tire-road forces and sideslip angle," *IEEE/ASME Trans. Mechatronics*, vol. 16, no. 4, pp. 601–614, Aug. 2011.

[26] L. R. Ray, "Nonlinear state and tire force estimation for advanced vehicle control," *IEEE Trans. Control Syst. Technol.*, vol. 3, no. 1, pp. 117–124, Mar. 1995.

[27] J. Matuško, I. Petrović, and N. Perić, "Neural network based tire/road friction force estimation," *Eng. Appl. Artif. Intell.*, vol. 21, no. 3, pp. 442–456, Apr. 2008.

[28] J. Kim, "Identification of lateral tyre force dynamics using an extended Kalman filter from experimental road test data," *Control Eng. Practice*, vol. 17, no. 3, pp. 357–367, Mar. 2009.

[29] W. Cho, J. Yoon, S. Yim, B. Koo, and K. Yi, "Estimation of tire forces for application to vehicle stability control," *IEEE Trans. Veh. Technol.*, vol. 59, no. 2, pp. 638–649, Feb. 2010.

[30] H. B. Pacejka, *Tyre and Vehicle Dynamics*. Oxford, U.K.: Butterworth-Heinemann, 2002.

[31] G. A. MacDonald, "A review of low cost accelerometers for vehicle dynamics," *Sens. Actuators A, Phys.*, vol. 21, no. 1–3, pp. 303–307, Feb. 1990.

[32] U. Maeder and M. Morari, "Attitude estimation for vehicles with partial inertial measurement," *IEEE Trans. Veh. Technol.*, vol. 60, no. 4, pp. 1496–1504, May 2011.

[33] K. J. Astrom and B. Wittenmark, *Adaptive Control*. Reading, MA, USA: Addison-Wesley, 1995.

[34] M. Choi, J. Oh, and S. Choi, "Linearized recursive least square methods for real-time identification of tire-road friction coefficient," *IEEE Trans. Veh. Technol.*, vol. 62, no. 7, pp. 2906–2918, Sep. 2013.

[35] MTS Systems, Swift 30 Sensor Product Information, 2008.

[36] J. Villagra, B. d'Andréa-Novel, M. Fliess, and H. Mounier, "A diagnosis-based approach for tire-road forces and maximum friction estimation," *Control Eng. Practice*, vol. 19, no. 2, pp. 174–184, Feb. 2011.

[37] J. Ryu and J. C. Gerdes, "Integrating inertial sensors with global positioning system (GPS) for vehicle dynamics control," *J. Dyn. Syst., Meas., Control*, vol. 126, no. 2, pp. 243–254, Aug. 2004.

[38] S. H. You, J. O. Hahn, and H. Lee, "New adaptive approaches to real-time estimation of vehicle sideslip angle," *Control Eng. Practice*, vol. 17, no. 12, pp. 1367–1379, Dec. 2009.

[39] L. Imsland *et al.*, "Vehicle velocity estimation using nonlinear observers," *Automatica*, vol. 42, no. 12, pp. 2091–2103, Dec. 2006.

Chang-Sei Kim (M'14) received the B.S. degree from Pusan National University, Busan, Korea, in 1998; the M.S. degree from Seoul National University, Seoul, Korea, in 2000; and the Ph.D. degree in mechanical engineering from Pusan National University in 2011.

He is currently a Research Associate with the University of Maryland, College Park, MD, USA. His research interest is modeling and control application to biomedical systems and industrial automation.

Jin-Oh Hahn (M'08) received the B.S. and M.S. degrees in mechanical engineering from Seoul National University, Seoul, Korea, in 1997 and 1999, respectively, and the Ph.D. degree in mechanical engineering from Massachusetts Institute of Technology, Cambridge, MA, USA, in 2008.

He is currently an Assistant Professor with the Department of Mechanical Engineering, University of Maryland, College Park, MD, USA. His current research interests include dynamical systems and the controls approach to health monitoring, diagnostics, and maintenance of dynamic systems.

Dr. Hahn received the Young Investigator Program Award from the Office of Naval Research in 2014 and the Young Investigator Grant Award from the Korean–American Scientists and Engineers Association in 2013.

Keum-Shik Hong (S'87–M'91–SM'10) received the B.S. degree from Seoul National University, Seoul, Korea, in 1979; the M.S. degree from Columbia University, New York, NY, USA, in 1987; and the M.S. degree in applied mathematics and the Ph.D. degree in mechanical engineering from the University of Illinois at Urbana-Champaign, Urbana, IL, USA, in 1991.

He is currently with the Department of Mechanical Engineering, Pusan National University, Busan, Korea. His current research interests include brain–computer interfaces, nonlinear systems theory, adaptive control, and distributed parameter systems control.

Dr. Hong has received many awards, including the 2007 Presidential Award of Korea.

Wan-Suk Yoo received the B.S. degree from Seoul National University, Seoul, Korea, in 1976; the M.S. degree from Korea Advanced Institute of Technology, Daejeon, Korea, in 1978; and Ph.D. degree in mechanical engineering from The University of Iowa, Ames, IA, USA, in 1985.

He is currently with the Department of Mechanical Engineering, Pusan National University, Busan, Korea. His major research areas are flexible multibody dynamics and vehicle dynamics.

Dr. Yoo was the President of the Korean Society of Mechanical Engineers in 2011 and has been a Fellow of the American Society of Mechanical Engineers since 2004.